Volume 16
Number 39
21 October 2025
Pages 17973–18462

Chemical Science

rsc.li/chemical-science

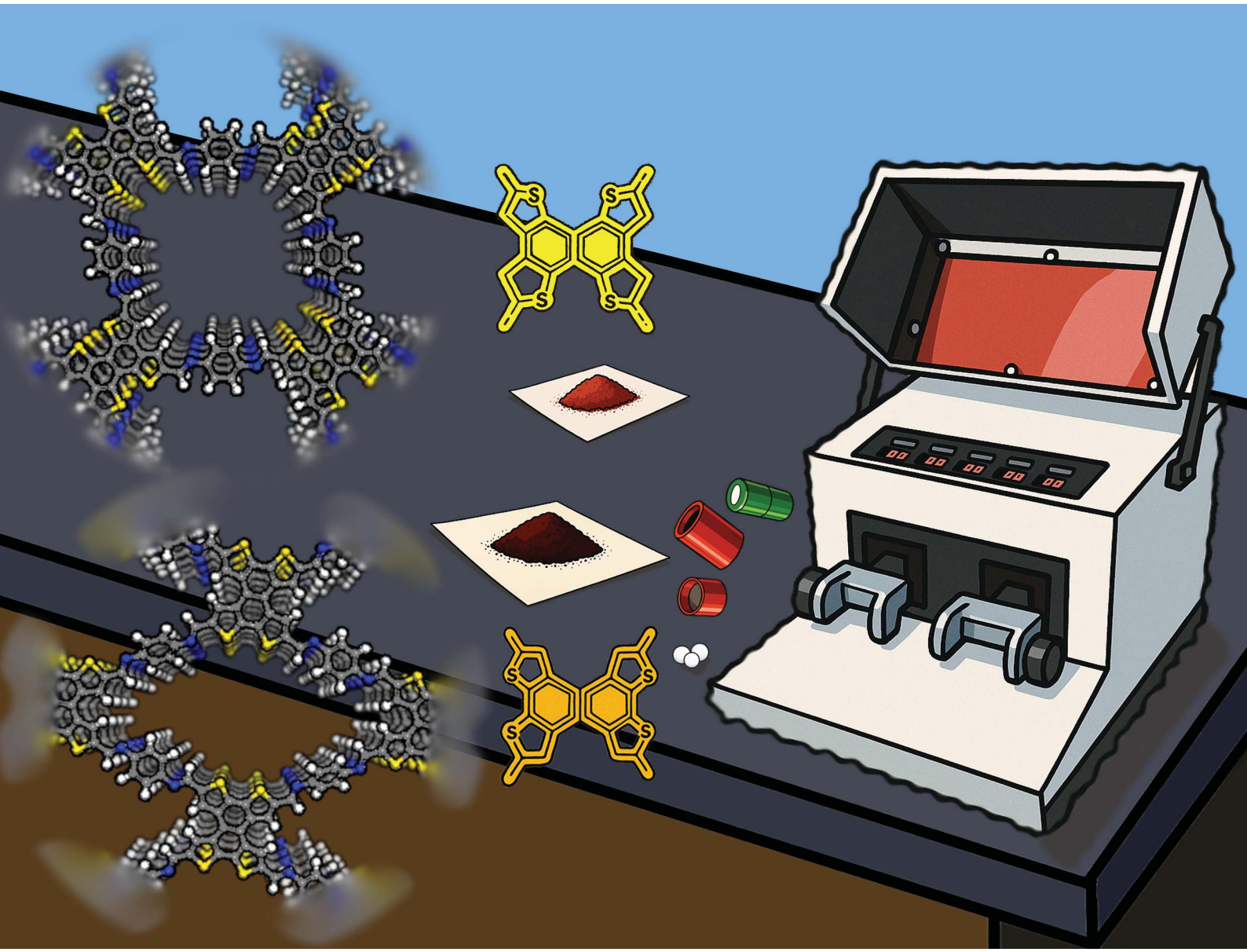

ISSN 2041-6539

ROYAL SOCIETY OF CHEMISTRY

EDGE ARTICLE

Dmytro F. Perepichka *et al.*

Mechanochemical synthesis of π-conjugated naphthotetrathiophene-based covalent organic frameworks and their post-modification *via* the Doebner reaction

15 YEARS ANNIVERSARY

Chemical Science

ROYAL SOCIETY OF CHEMISTRY

EDGE ARTICLE

View Article Online
View Journal | View Issue

Cite this: *Chem. Sci.*, 2025, **16**, 18101

All publication charges for this article have been paid for by the Royal Society of Chemistry

Mechanochemical synthesis of π-conjugated naphthotetrathiophene-based covalent organic frameworks and their post-modification *via* the Doebner reaction

Mohammad Hossein Gohari, [a] Pegah Ghamari,[ab] Ehsan Hamzehpoor,[a] Farshid Effaty, [acd] Tomislav Friščić [ad] and Dmytro F. Perepichka *[a]

We report that mechanochemistry enables the synthesis of new π-conjugated covalent organic frameworks (COFs) based on naphthotetrathiophenetetracarbaldehydes **2TTN** and **3TTN**, expanding the scope of COF structures with two new isomeric tetradentate nodes. While recent studies have explored COF isomerism by varying bidentate linkers to tune electronic properties, the impact of *node* isomerism remains largely unexplored. Here, we overcome these limitations using mechanochemistry to access COFs based on insoluble fused polycyclic heteroaromatic monomers. These COFs exhibit broad absorption across the visible spectrum with **3TTN** COFs showing a red-shifted absorption compared to their **2TTN**-counterparts. Microwave-assisted post-modification of COFs *via* the Doebner reaction converts imine into quinoline linkages, enhancing the chemical stability of the COF. We explore the effect of the node structure (**2TTN** *vs.* **3TTN**) and the network connectivity (phenylenediamine, biphenylenediamine and biquinoline) on optical band-gaps of the COFs. All COFs have shown a marked increase in electrical conductivity, by 6 orders of magnitude, upon p-doping with iodine. Quinoline-linked COFs showed proton conductivity up to 1.2×10^{-3} S cm^{-1} at 60 °C and a relative humidity of 75%. This work suggests new possibilities for electronic modulation in COFs through *node* isomerism and offers a sustainable route to robust, tunable, heteroaromatic frameworks.

Received 15th June 2025
Accepted 1st September 2025

DOI: 10.1039/d5sc04390e

rsc.li/chemical-science

Introduction

Covalent organic frameworks (COFs) are crystalline porous two-dimensional (2-D) or three-dimensional polymers with growing applications in materials science,[1–3] including chemical separation, proton conduction, sensing, and energy storage, due to their structural tunability.[1,4,5] Their predictable chemistry allows for precise tuning of optical properties.[6,7] 2-D COFs with covalently linked subunits and π-stacking interlayers can support efficient charge transfer,[8] making them suitable for electronic device applications. Although the tunability of crystalline frameworks is a fundamental motivation in COF research, the properties of these materials frequently emerge from serendipitous discoveries rather than rational design.[9–13] Studying the effect of isomerism in COFs has recently attracted attention as a means for uncovering structure–property relationships in COFs without perturbing their symmetry and the overall topology of the framework. While a significant effort was focused on isomeric linkages,[6,14–21] the influence of *node* isomerism on COF properties is almost unexplored.[22–24]

Thiophene stands out as the most common building block in conjugated polymers and oligomers with many thousands of thiophene-based structures explored for their semiconducting properties.[25,26] Incorporation of thiophene in COFs promises the realization of nanoporous materials with highly efficient charge transport and useful semiconducting, photocatalytic and related applications.[27–31] Nonetheless, among hundreds of different COFs developed over the last two decades, only a handful are based on thiophene nodes and linkers (Scheme 1a, b and SI Table S6).[1,6,28,32–41] The wide development of thiophene based 2D-COFs is hindered by several challenges. One is the lower symmetry of thiophene linkers (C_{2v}) compared to the commonly used phenylene (C_{2h}) which can introduce disorder in the framework.[38]

COFs with Lieb lattices are of particular interest as the unique band structure of such a lattice can result in unusual electronic and magnetic properties including ferromagnetism or superconductivity.[42,43] Creation of such a lattice requires

[a]*Department of Chemistry, McGill University, 801 Sherbrooke St.W., Montreal, H3A 09B, Canada. E-mail: dmytro.perepichka@mcgill.ca*

[b]*Centre Énergie, Matériaux et Télécommunications, Institut National de la Recherche Scientifique, Varennes, Québec J3X 1S2, Canada*

[c]*Department of Chemistry and Biochemistry, Concordia University, 7141 Sherbrooke St. West, Montreal, QC, H4B 1R6, Canada*

[d]*School of Chemistry, University of Birmingham, Edgbaston, Birmingham, B15 2TT, UK*

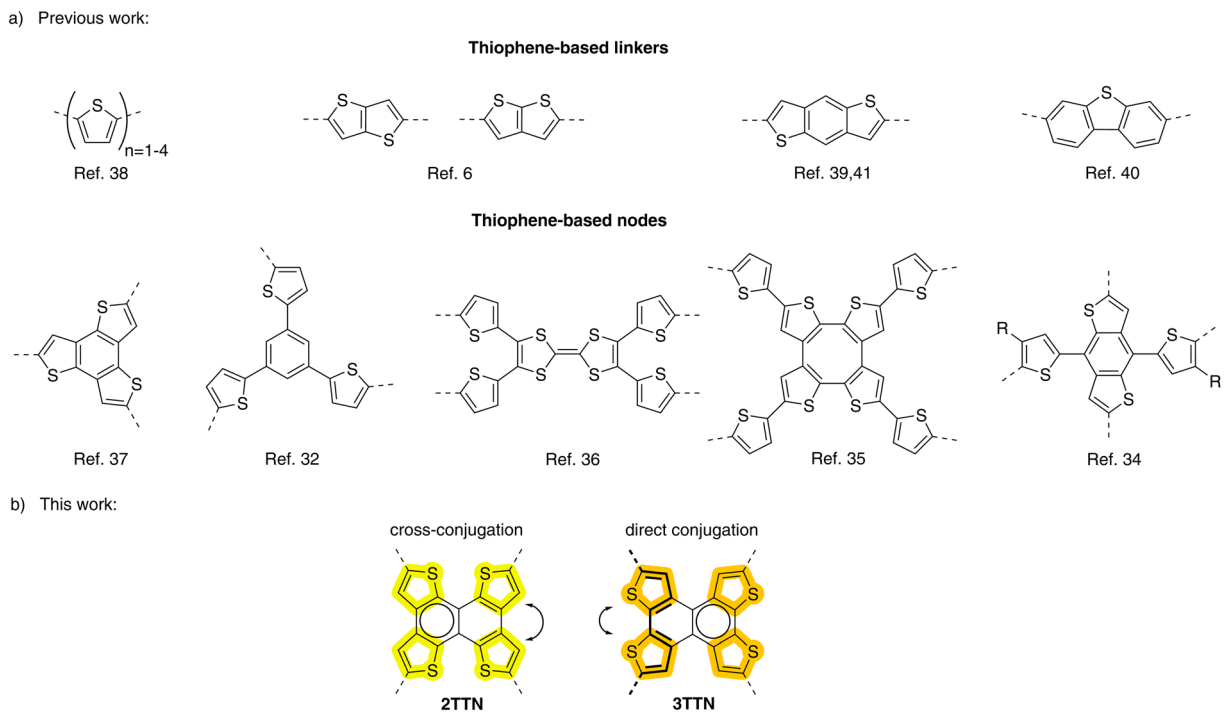

Scheme 1 (a) Thiophene-containing linkers and nodes used in reported COFs. (b) New isomeric naphthotetrathiophene (TTN) nodes reported here.

tetrafunctional nodes but a few such COFs have been realized to date and in most cases their π-conjugation is limited by dihedral twist between the node and the linker.[44–46] In this regard, we reasoned that the planar isomeric naphthotetrathiophene **2TTN** and **3TTN** nodes would be of significant interest for the synthesis of highly conjugated COFs (Scheme 1).

However, planarization and extension of polycyclic aromatic cores, such as in **2TTN** and **3TTN**, often result in poor solubility, which complicates the solvothermal COF synthesis. In principle, this challenge can be tackled by applying mechanochemical solvent-free methods which could also shorten the reaction time, lower the reaction temperature, and dramatically reduce the amount of generated waste, compared to the traditional solvothermal synthesis.[47] Since Banerjee *et al.* first introduced the mechanosynthesis of COFs *via* manual grinding,[48] this strategy has gained significant attention in the field.[49] Various mechanochemical techniques have subsequently been applied for the synthesis of COFs, including ball milling,[50,51] screw extrusion,[52] and resonant acoustic mixing (RAM).[53] The majority of mechanochemically synthesized COFs are based on Schiff-base condensation reactions,[48,50–52,54–63] although other linkages such as boroxine[53] and triazine[64] have also been successfully explored using similar methodologies. Despite these significant advancements, only a small set of nodes has been used in mechanochemically synthesized COFs to date (Table S7).[48,50,53,57–60,64–66] A key challenge is that mechanochemically synthesized COFs typically exhibit low crystallinity compared to solvothermal products.[48,51,54–56,64,67] Furthermore, all of them rely on soluble precursors that can afford the same COFs (usually with superior crystallinity) *via* conventional solvothermal methods.

In this study, we introduce two isomeric tetrafunctional naphthotetrathiophene monomers, **2TTN-CHO** and **3TTN-CHO**, and use them in the mechanochemical synthesis of COFs with varied linkers (Scheme 2). We investigate how the connectivity of their thiophene units and the linker influence the photophysical properties of the resulting COFs and further investigate a Doebner reaction post-modification to transform imine-linked COF **2TTN-COF2** into quinoline-linked **2TTN-COF2-Q** COF improving the chemical stability and shrinking the band gap by 0.4 eV. The **2TTN-COF2-Q** COF shows a proton conductivity of 3×10^{-4} S cm^{-1} at room temperature and relative humidity (RH) of ~75%.

Results and discussion

Synthesis and characterization

To construct the target thiophene-based COFs, we have synthesized two isomeric tetrathienonaphthalene monomers, **2TTN-CHO** and **3TTN-CHO**. A lithiation-formylation sequence on the tetrathienylethylenes **2TTE** and **3TTE** (Scheme 2, S1 and S2) affords the precursor aldehydes **2TTE-CHO**[68] and **3TTE-CHO**. Despite the strongly electron-withdrawing aldehyde groups, iodine-assisted photooxidative cyclization of **2TTE-CHO** and **3TTE-CHO** in the presence of methyloxyrane as an HI scavenger[69] resulted in **2TTN-CHO** (91%) and **3TTN-CHO** (50%), akin to those reported for unsubstituted **2TTE**[70] and **3TTE**.[71] The cyclized aldehydes precipitate from the reaction solution due to their low solubility (<10^{-4} M in DMF for **2TTN-CHO** at room temperature) and were washed with organic solvents (DCM and methanol) and vacuum dried to afford pure solids (confirmed by ^{1}H NMR at 120 °C).

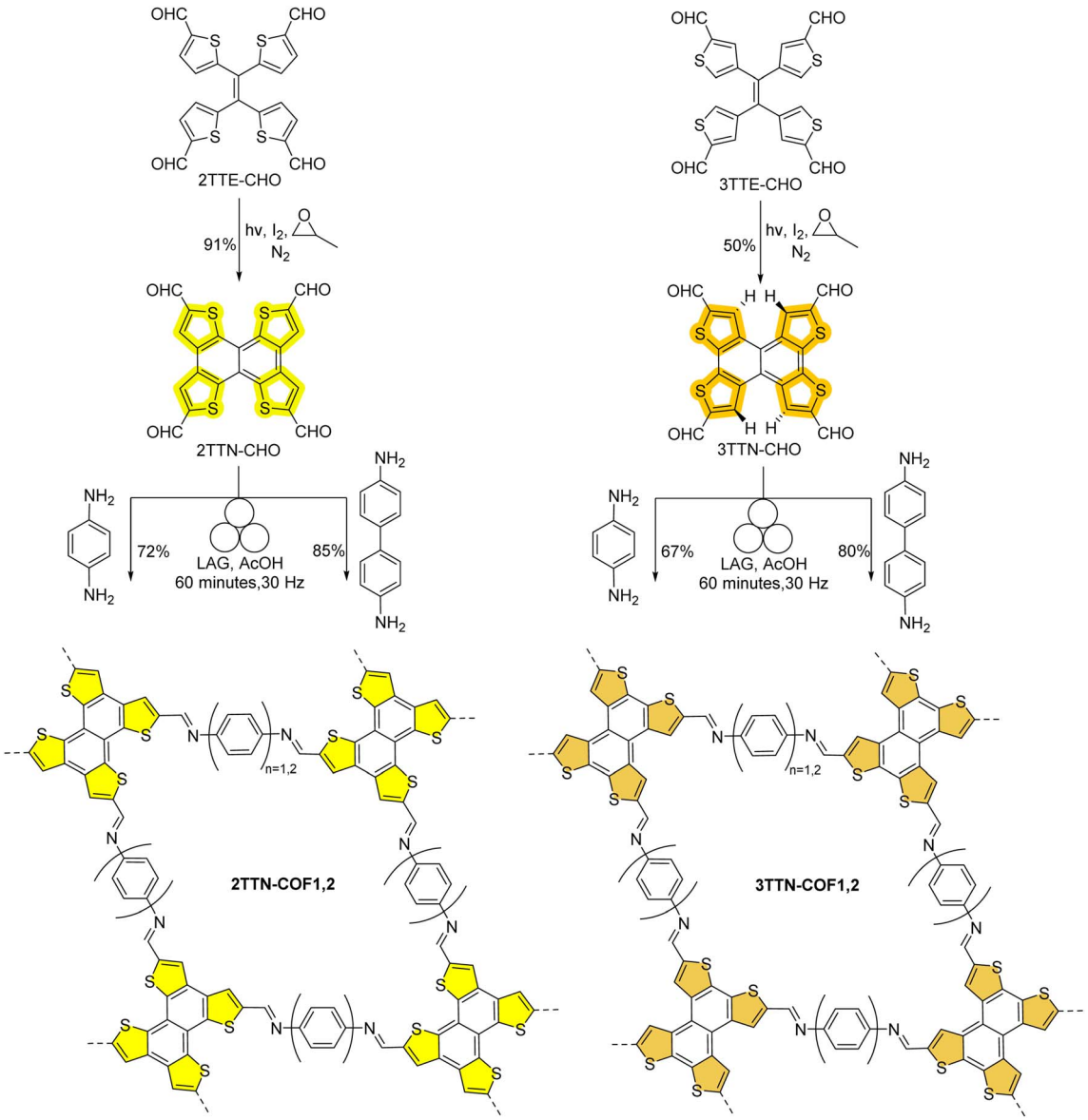

Scheme 2 Synthesis of TTN nodes and mechanochemical synthesis of naphthotetrathiophene-derived COFs.

Our initial attempts at solvothermal synthesis of **2TTN-COFs** and **3TTN-COFs** from the corresponding aldehydes with 1,4-diaminobenzene resulted in poor conversions as evidenced by the remaining highly insoluble, crystalline aldehyde monomers (Fig. S4a). We thus turned to mechanochemical polymerization using a ball-milling method.

The reaction was optimized for the copolymerization of **2TTN-CHO** with 1,4-diaminobenzene to construct **2TTN-COF1** in zirconia milling assembly (a 15 mL volume jar and a 2.6 g/10 mm diameter ball) (Table S1a). Using Lewis acid $Sc(OTf)_3$ as a catalyst with 1,4-dioxane as the liquid additive only yielded a COF with low crystallinity. Changing the catalyst to acetic acid improved the crystallinity but residual diffraction peaks of the aldehyde could still be observed even at longer milling times (Table S1a, entry 4). Increasing the milling frequency from 25 to 30 Hz improved the crystallinity and conversion as assessed by the PXRD and IR analyses (Table S1a, entry 5). Increasing the amount of the catalyst and liquid additive (the ratio of liquid additive to reaction mixture weight, $\eta = 2.0$–3.5 μL mg^{-1}) and replacing the liquid additive with THF had negligible effects on the crystallinity and the conversion in 60 minutes, which turned out to be the best (optimized) condition (Table S1a, entry 7). A lower ratio ($\eta = 1.8$ μL mg^{-1}), closer to that used in mechanochemical liquid-assisted grinding (LAG)[72], resulted in slightly higher crystallinity and conversion (Table S1a, entries 2, 5 and 9); however, these conditions proved less reproducible. The need for a higher amount of liquid could be attributed to trapping of the solvent in the pores of the formed COF.

Increasing the milling time from 60 minutes to 90 minutes improved the conversion of aldehyde groups as shown by FTIR (Table S1a, entry 9 and Fig. S18b). However, the accessible surface area of the COFs is reduced from 493 m^2 g^{-1} to 251 m^2

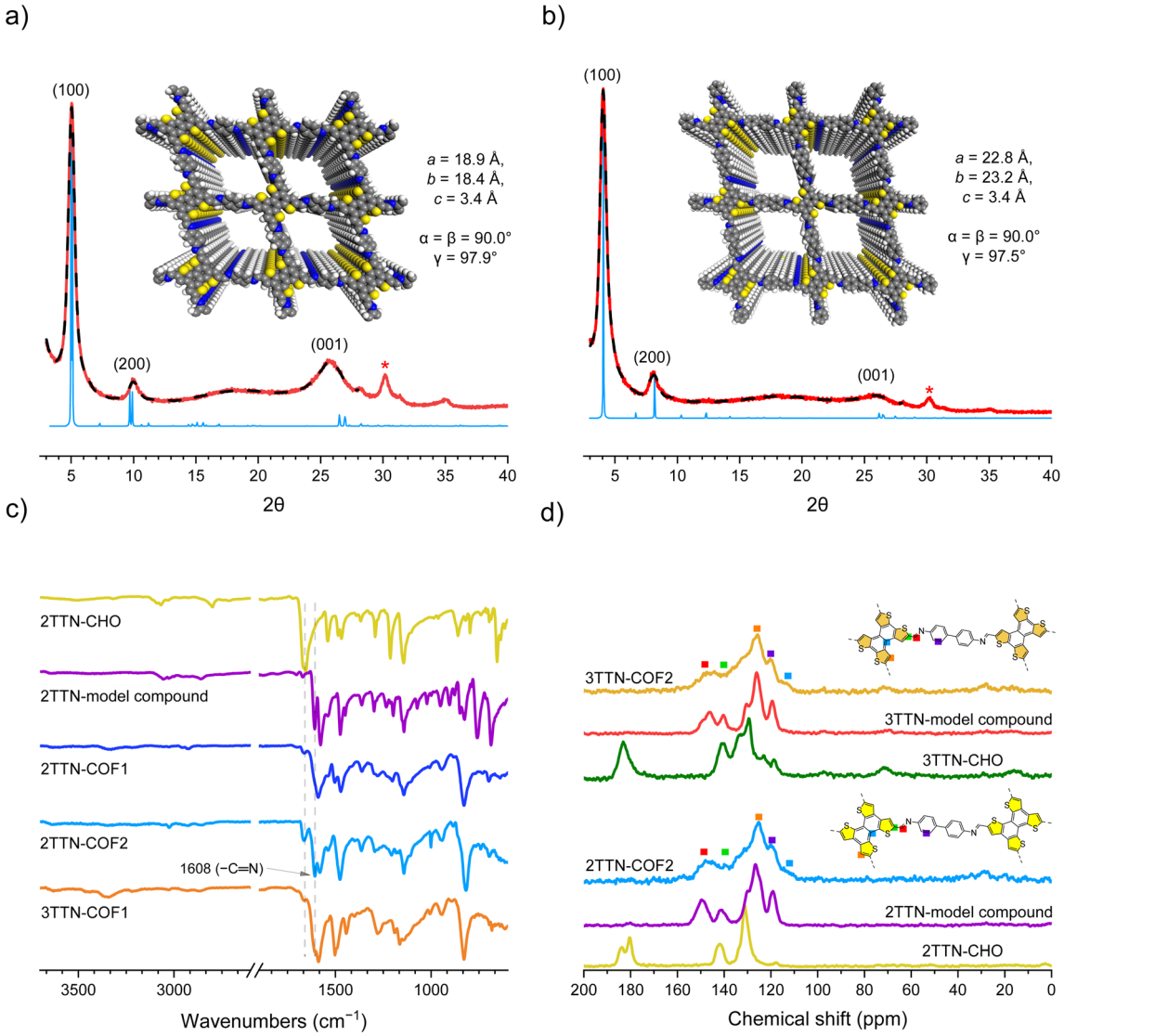

Fig. 1 PXRD patterns of (a) **2TTN-COF1** powder (observed (red), refined (dashed) and simulated AA stacking (blue), $R_p = 2.15\%$, $R_{wp} = 2.74\%$), (b) **2TTN-COF2** (observed (red), refined (dashed) and simulated AA stacking (blue), $R_p = 2.55\%$, $R_{wp} = 3.45\%$), and the inset shows the simulated structures. Full Width at Half Maximum (FWHM) is 0.57° and 0.56° for **2TTN-COF1** and **2TTN-COF2**, compared to 0.85° and 0.63° for **3TTN-COF1** and **3TTN-COF2** for 100 plane peaks, respectively (Fig. S3). (c) IR spectra of aldehydes, the model compound, and COF powders showing the imine linkages at 1608 cm^{-1} and residual aldehyde peak at 1660 cm^{-1}, and (d) comparison of ^{13}C NMR starting materials, model compounds and COF powders measured at (CP-MAS, 13 kHz). The peaks marked by * in (a) and (b) are due to trace amounts of zirconia leaching from jars (≤0.5% based on X-ray photoelectron spectroscopy (XPS), Fig. S6b, S9–S13).

g^{-1}, possibly due to pore collapse and/or pore blockade due to interlayer shift (Fig. S26g).[53] Using softer milling materials, such as steel and Teflon, instead of zirconia resulted in incomplete polymerization as indicated by the presence of the aldehyde precursors by FTIR and PXRD (Fig. S6a, S18a and Table S1a, entries 12–18). The COF powders from the optimized condition were washed thoroughly with polar solvents (DCM, methanol, and acetone), filtered, and purified by Soxhlet extraction with THF.

Under the optimized reaction conditions, we also reacted **3TTN-CHO** with 1,4-diaminobenzene, resulting in the formation of **3TTN-COF1** (Table S1b), as well as reacting both aldehyde precursors with benzidine, yielding **2TTN-COF2** and **3TTN-COF2**, respectively. To aid the structural characterization of COFs, model compounds were synthesized from **2TTN-CHO**, **3TTN-CHO** and aniline, by both solvothermal and mechanochemical methods.

The PXRD analysis of **2TTN-COF1** revealed a crystalline structure with Bragg reflections at $2\theta = 5.0°$ and 9.9°, corresponding to the (100) and (200) planes (Fig. 1a). A broad peak at $2\theta \approx 26°$ was attributed to the (001) plane, indicating weak long-range order along the crystallographic c direction with an interlayer spacing of ~3.4 Å. Pawley refinement suggests a monoclinic unit cell with $a = 18.9$ Å, $b = 18.4$ Å, $c = 3.4$ Å, $\alpha = \beta = 90°$, and $\gamma = 97.9°$. The PXRD analysis of **2TTN-COF2** showed Bragg reflections at $2\theta = 4.1°$ and 8.1° (Fig. 1b and S3b).

For **3TTN-COF1**, the first reflection appeared at $2\theta = 5.9°$ (100), and the unit cell was refined to $a = 17.9$ Å, $b = 18.6$ Å, $c = 3.4$ Å, $\alpha = \beta = 90°$, and $\gamma = 114.2°$ (Fig. S3c). PXRD patterns of **3TTN-COF2** revealed peaks at $2\theta = 4.8°$ and 8.7° (Fig. S3d). The simulated diffraction patterns for the DFT-optimized unit cell closely matched the experimental data, reproducing both the reflection positions and the relative intensities suggesting an eclipsed (AA) interlayer orientation for all COFs (Fig. S3).

The crystal structures of the unsubstituted **2TTN** and **3TTN**[71,73] show that the former is completely planar while the latter exhibits a small twist of ~7°, brought about by steric repulsion between hydrogen atoms in the bay area. This out-of-place distortion may explain the slightly lower crystallinity of **3TTN** COFs compared to **2TTN** COFs. Scherrer analysis of the (100) reflection width suggests a crystal coherence length of ~14 nm for both **2TTN-COF1** and **2TTN-COF2** and lower values of ~9 nm for **3TTN-COF1** and ~13 nm for **3TTN-COF2**.

The IR spectrum of **2TTN-COF1** displays a characteristic C=N stretch at ~1608 cm^{-1} (Fig. 1c and S17). The dramatic decrease in the aldehyde C=O stretch indicates that the reaction is nearly complete within 60 minutes of milling. Solid-state cross-polarization magic-angle-spinning (CP-MAS) ^{13}C NMR spectroscopy confirms the complete imine formation as indicated by the C=N peak at ~150 ppm and the disappearance of aldehyde groups at ~190 ppm (Fig. 1d and S28).

The elemental composition analysis obtained from X-ray photoelectron spectroscopy (XPS) is in good agreement with the expected elemental composition for all 4 COFs (Fig. S9–S13). For instance, for **2TTN-COF1**, the obtained elemental composition is 80.0 ± 0.5%, 9.1 ± 0.7%, and 7.4 ± 0.6% for C, N, and S while the expected values are 81.0%, 9.5%, and 9.5%, respectively. XPS also shows ~3.5% of oxygen present on the COF surface which we attribute to unreacted aldehyde groups, possibly chemisorbed water (as hemiaminal) and a small amount of ZrO_2 (0.13%) from the milling jar (Fig. S9 and S10, SI Section 12.2).

Brunauer–Emmett–Teller (BET) analysis of the 77 K nitrogen sorption measurements of vacuum-activated COFs (10^{-3} torr, 120 °C, 24 h) suggests a relatively low surface area of 311 $m^2\ g^{-1}$ for **2TTN-COF1** (theoretical 1584 $m^2\ g^{-1}$, Fig. S26a). Owing to its larger unit cell, **2TTN-COF2** exhibits a higher surface area of 493 $m^2\ g^{-1}$ (theoretical: 1793 $m^2\ g^{-1}$). However, both **3TTN** COFs showed a much lower surface area of 23–90 $m^2\ g^{-1}$ (Fig. S26), which is in line with their lower crystallinity. We attribute this low surface area of all four COFs to the interlayer slippage/pore collapse during milling.[48] The pore size distribution obtained from the quenched-solid density functional theory (QS-DFT) of the N_2 isotherm data for **2TTN-COF1** corresponds closely to the micropore dimensions expected for the COF (19 Å) with contributions of mesopores at ~35–50 Å (Fig. S26h).

The scanning electron microscopy (SEM) image shows micrometer-sized particles, with occasional plates reaching up to 100 μm for **2TTN-COF1** and **3TTN-COF1** (Fig. S27). Thermogravimetric analysis (TGA) confirms that all COFs are stable up to at least 300 °C, with the highest stability observed for **2TTN-COF1** with T_{dec}^{95} ~ 440 °C (Fig. S20).

Postmodification of COFs *via* the Doebner reaction

Imine COFs exhibit limited hydrolytic stability and limited π-electron delocalization due to the polarity of the C=N linkage.[74] Various post-synthetic modification strategies have been developed to improve the stability and π-conjugation of imine COFs.[75,76] These strategies often involve harsh conditions.[77] Notably, the Doebner reaction improves chemical stability and introduces functionality for various applications under mild reaction conditions.[78,79] The combination of the electron-rich TTN node with the electron-withdrawing quinoline linkage is expected to lower the band gap compared to that of its imine-linked COFs.

The COF **2TTN-COF2**, which exhibits the highest crystallinity and largest pores in this series, was selected for post-modification. Using a modified Doebner reaction condition[78] (Table S8), the imine-linked **2TTN-COF2** was reacted with pyruvic acid at 120 °C in an air atmosphere to obtain quinoline-linked **2TTN-COF2-Q** in 75% yield (Scheme 3). The addition of small amounts of the free benzidine linker was essential to

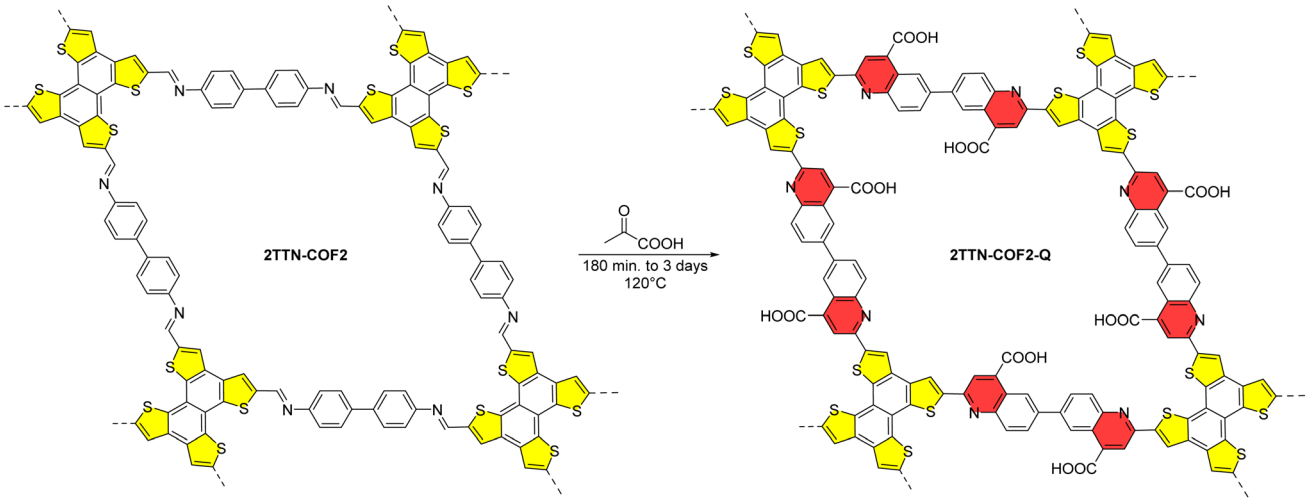

Scheme 3 Post-synthetic modification of 2TTN-COF2 for synthesis of quinoline-linked 2TTN-COF2-Q.

prevent the hydrolysis of imine bonds during the reaction, which otherwise leads to formation of the aldehyde monomer observed in the PXRD pattern of the post-modified COF (Fig. S4b).

Unlike imine-linked TTN COFs, which undergo complete dissolution by acid catalyzed aminolysis with hexylamine[80] (Fig. S2), quinoline links are completely stable under these conditions. To assess the efficiency of the post-modification, the resulting **2TTN-COF2-Q** was reacted with hexylamine to digest the unconverted imine-linked domains. Such aminolysis of **2TTN-COF2-Q** prepared under solvothermal conditions (over 3 days) resulted in 67% mass retention for **2TTN-COF2-Q**. The conversion yield can be increased by performing the Doebner reaction under solvent-free conditions (77% mass retained after aminolysis, SI Section 5) but with a significant loss of crystallinity (Fig. S7). On the other hand, this reaction can be accelerated (3 h) using microwave-assisted heating[81,82] while maintaining the crystallinity (Fig. S7) and achieving comparable conversion (57% mass retention after aminolysis).

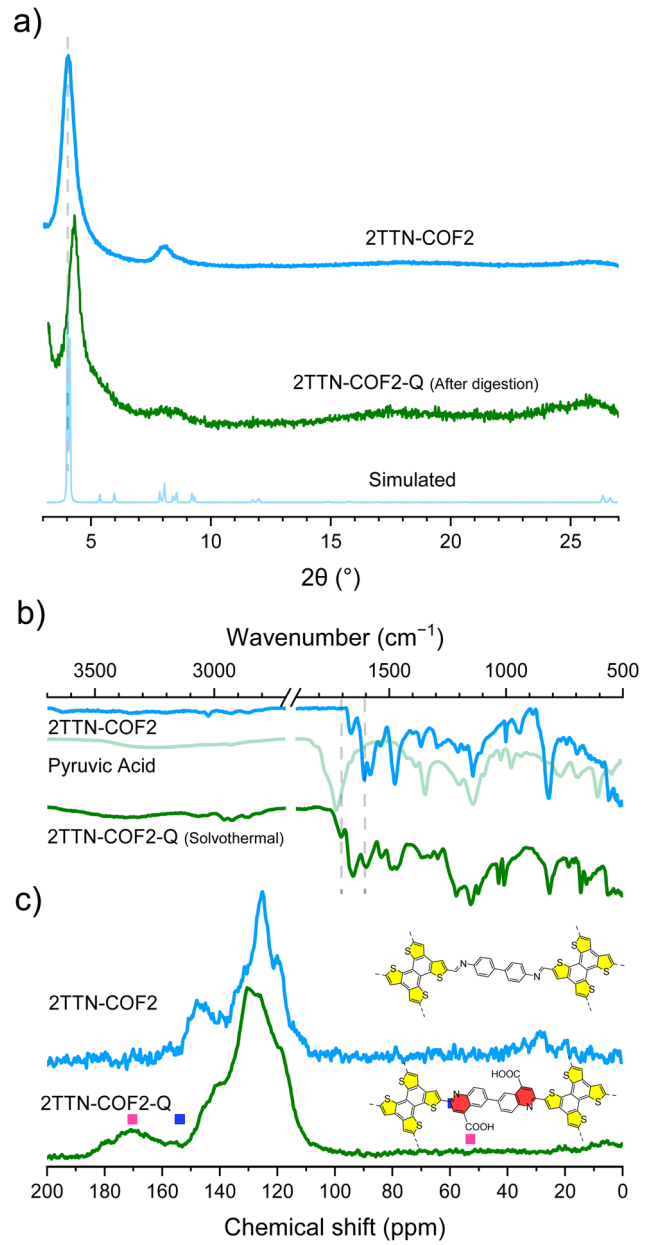

Fig. 2 (a) Experimental (blue) PXRD pattern of **2TTN-COF2**, and experimental (green, background corrected) and simulated (light blue, AA stacking) PXRD patterns of **2TTN-COF2-Q** synthesized solvothermally (after digestion). (b) IR spectra of **2TTN-COF2-Q**, compared to those of **2TTN-COF2** and pyruvic acid. (c) CP/MAS ^{13}C NMR spectra of **2TTN-COF2** and **2TTN-COF2-Q** measured at 13 kHz.

The IR spectra of **2TTN-COF2-Q** COFs (Fig. 2b and S19) display characteristic peaks at 1704 cm^{-1} corresponding to the carboxylic group. The higher relative intensity of the carboxylic peak in the solvent-free approach compared to solvothermal and microwave-assisted, agrees with the higher conversion of the imine-linked COF in this approach (Fig. S19). The CP-MAS ^{13}C NMR spectrum shows an additional peak at ~170 ppm corresponding to the carboxylic group (Fig. 2c and S29). The XPS analysis of the **2TTN-COF2-Qs** shows an expected increase in the amount of oxygen (11.8%) and an overall good match of elemental composition with theoretical values (with deviations ≤1.3%, Table S2).

The surface area of **2TTN-COF2-Q** (solvothermal) is reduced to ~190 $m^2\ g^{-1}$, which is in agreement with the reduced pore size of the quinoline-linked COF (SI Section 12.8). Thermogravimetric analysis (TGA) of post-modified COFs shows lower thermal stability compared to imine-linked COFs (Fig. S20). TGA-IR measurements of the Doebner post-modified COF confirm that the significant mass loss observed between 180 °C and 500 °C is attributed to CO_2 evolution from decarboxylation. The measured mass loss of 14.7% in this temperature range aligns well with the theoretical 17% mass loss calculated for the conversion of the 4-carboxyl-quinoline-linked COF to the quinoline-linked COF (Fig. S21).

Photophysical characterization

The optical properties of the COF powders were analyzed using diffuse reflectance spectroscopy (DRS), and their direct optical band gaps (E_g) were determined from Tauc plots (Fig. S22b). The as-prepared TTN COFs exhibited broad absorption across the visible spectrum (Fig. 3a and S22). The absorption band of **3TTN-COF1** is red-shifted compared to that of **2TTN-COF1** by 20 nm, which corresponds to a decrease in the band gap from 1.89 eV to 1.81 eV. This effect is likely a result of the enhanced intra-sheet electron delocalization *via* **3TTN** *vs.* **2TTN** core, which can be rationalized in the context of direct conjugation through the bithiophene moiety in **3TTN** *vs.* cross-conjugation in **2TTN** (Scheme 1b). Indeed, DFT calculations (B3LYP/6-31G(d)) on 2-D COF monolayers reveal a narrower band gap for **3TTN-COF1** (2.78 eV) compared to **2TTN-COF1** (3.35 eV), despite the reduced planarity of **3TTN-COF1**. Furthermore, **3TTN-CHO** also shows a red-shifted emission compared to **2TTN-CHO** in solution (Fig. S8d). On the other hand, a blue-shifted absorption of the biphenylene-linked **2TTN/3TTN-COF2** *vs.* phenylene-linked **2TTN/3TTN-COF1** can be attributed to the twist in the biphenyl linker which limits the π-conjugation.[83,84]

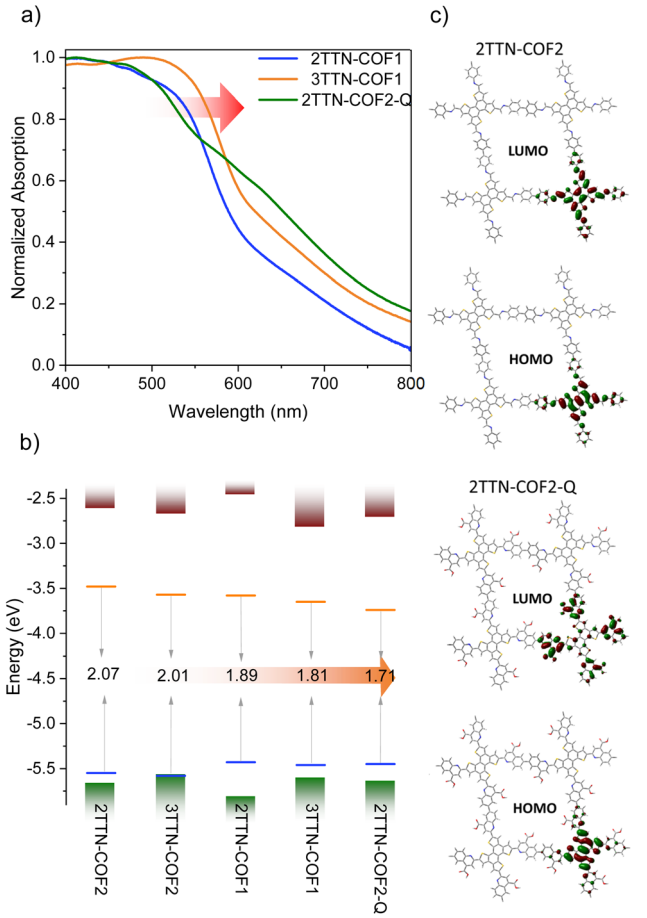

Fig. 3 (a) Diffuse reflectance spectra of the COF powders. (b) DFT-calculated (B3LYP/6-31G(d), red and green rectangles) and experimental (blue lines: PESA; orange lines: PESA + optical band gap) electronic levels of the COFs, and (c) DFT calculated orbital topologies for 2TTN-COF2 (top) and 2TTN-COF2-Q (bottom).

Converting the imine linker to a quinoline moiety results in a significant band gap contraction from 2.07 eV in **2TTN-COF2** to ~1.7 eV in **2TTN-COF2-Q** (Fig. S22b) which is in line with narrower calculated band gaps for this COF. This is consistent with enhanced π-conjugation and donor–acceptor interactions. While both the HOMO and LUMO in **2TTN-COF2** are primarily localized on the TTN core, the LUMO in quinoline-linked **2TTN-COF2-Q** is mainly located on the electron withdrawing linkage leading to a reduced band gap (Fig. 3b, S14 and Table S3).

The ionization potentials (IPs) of the COFs were measured using Photoelectron Yield Spectroscopy in Air (PESA, Fig. 3c and S16). Phenylene-linked COFs showed slightly lower IPs (5.43 eV for **2TTN-COF1** and 5.46 eV for **3TTN-COF1**) than biphenylene-linked COFs (5.55 eV for **2TTN-COF2** and 5.58 eV for **3TTN-COF2**). Converting the imine links in **2TTN-COF2** to quinoline leads to a ~0.1 eV decrease in IP for **2TTN-COF2-Q** (5.45 eV), consistent with its lower band gap. A summary of the energy levels of the COFs is presented in Fig. 3b and Table S3.

Electronic and proton conductivity

The dc electrical conductivity of TTN COFs was evaluated in compressed pellets using a two-probe measurement. Pristine COFs exhibited very low conductivities of $10^{-10}\cdots10^{-11}$ S cm^{-1} (Fig. S30). Doping in iodine vapor overnight improved the conductivity by up to six orders of magnitude (Fig. 4a). Specifically, an electrical conductivity of 3.2×10^{-4} S cm^{-1} and 1.7×10^{-5} S cm^{-1} was measured for phenylene-linked **2TTN-COF1** and **3TTN-COF1**, respectively. A lower conductivity was found in biphenylene-linked **2TTN-COF2** and **3TTN-COF2** (7.6×10^{-5} S cm^{-1} and 4.1×10^{-6} S cm^{-1}, respectively), while biquinoline-linked **2TTN-COF2-Q** showed a slightly enhanced conductivity of 1.1×10^{-4} S cm^{-1} (Fig. S30).

The absorption of iodine-doped COFs is red-shifted compared to that of pristine samples, with a low-intensity tail extending far into the near-IR region (Fig. 4c and S23). Electron Spin Resonance (ESR) spectroscopy shows the emergence of a strong signal upon doping, attributed to radical cations

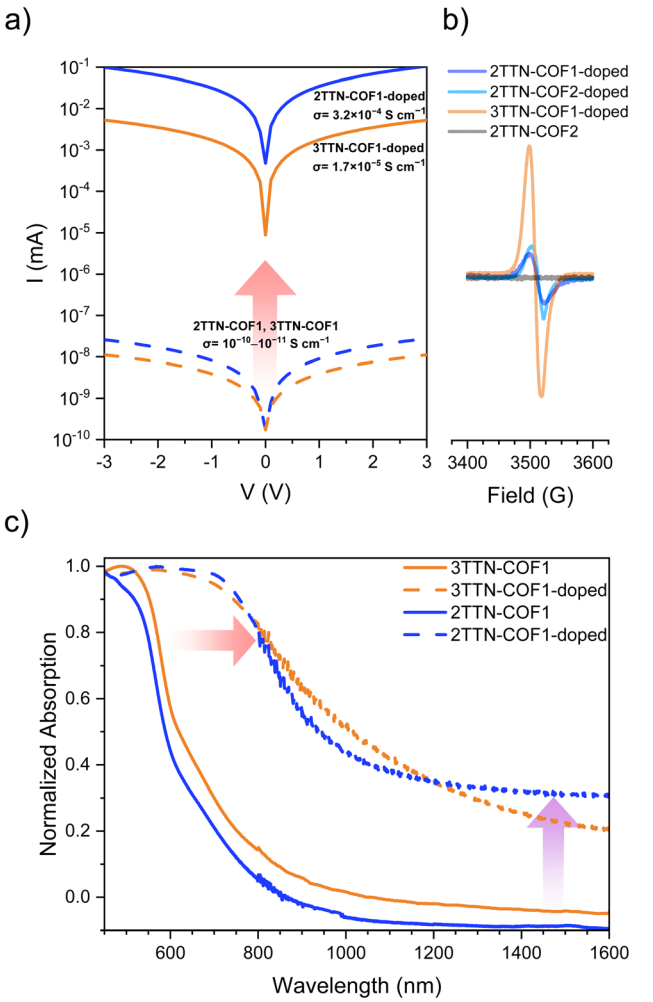

Fig. 4 (a) Comparison of the log scale of electrical conductivity measurements of pristine and I_2-doped 2TTN-COF1 and 3TTN-COF1; (b) EPR signal of pristine and I_2-doped COFs at room temperature in air; (c) diffuse reflectance spectra of the pristine and I_2-doped COF powders showing significant redshifts upon doping.

(Fig. 4b and S31). However, the measured spin concentration is rather low (0.2–0.3% for **2TTN-COF1** and **2TTN-COF2** and 1% for **3TTN-COF1**). It is likely that the relatively high ionization potentials (Fig. 3c) and possibly the instability of radical cations limit the generation of free carriers and thus the electrical conductivity of these COFs.

Considering the growing interest in proton-conducting COFs,[85–87] we evaluated the proton conductivity of **2TTN-COF2-Q** using electrochemical impedance spectroscopy (EIS) on compressed pellets doped with H_3PO_4, under both non-hydrous (vacuum-dried samples) and humid conditions (equilibrated overnight at RH ~75%). Analysis of the Nyquist plots revealed a reasonably high room-temperature proton conductivity of $\sim 1.4 \times 10^{-4}$ S cm^{-1} in the freeze-dried sample, but only a moderate increase to $\sim 3 \times 10^{-4}$ S cm^{-1} after humidification (Fig. S32). A further increase in proton conductivity to 1.2×10^{-3} S cm^{-1} was observed at 60 °C. These values are lower than 10^{-2} S cm^{-1} reported in a vinylene-linked triazine COF[87] under comparable conditions and the record $\sim 10^{-1}$ S cm^{-1} reported for a ketoenamine-linked azo-COF at saturated humidity (RH ≈ 98%) at higher temperature.[88] We speculate that the basicity of the quinoline nitrogen may increase the binding of protons in the COF cavity and limit the conductivity.

Conclusion

In summary we have introduced two new isomeric tetragonal π-conjugated naphthotetrathiophene isomers as cores for COF synthesis, and synthesized imine-linked COFs *via* mechanochemistry which was not readily accessible under typical solvothermal conditions. The synthesized COFs show high crystallinity with permanent porosity and optical band gaps ranging from 1.81 eV to 2.07 eV. We modified **2TTN-COF2** using the Doebner reaction under solvothermal conditions to yield quinoline linked **2TTN-COF2-Q** reducing the band gap of the COF by about 0.4 eV with a slight improvement in the conductivity of the COF and a significant improvement of chemical stability. Both experimental and DFT results show that the structural differences in the TTN-COFs lead to different π-conjugation and planarity, which significantly impact their optical and electronic properties. We also developed microwave-assisted Doebner post-modification synthesis of quinoline-linked COFs which significantly shortens the reaction time compared to the conventional solvothermal conditions. Due to the relatively high ionization potential ($\gtrsim$5.5 eV) of these COFs, only low charge carrier concentration (0.2–0.3%) can be introduced by doping with iodine. Nevertheless, such doping increases the electrical conductivity by 6 orders of magnitude (up to 3×10^{-4} S cm^{-1}) indicating pronounced charge transport properties of TTN-based COFs. Quinoline-linked COFs showed a proton conductivity of 1.2×10^{-3} S cm^{-1} at 60 °C and moderate RH (~75%). Our results showcase the advantages of mechanochemistry in providing straightforward access to COFs based on insoluble monomers, providing the opportunities for design of such materials based on large poly(hetero)cyclic building blocks with tailorable optoelectronic properties.

Author contributions

M. H. G. and D. F. P. conceived the project. M. H. G. synthesized, purified, and characterized TTN monomers and COFs. P. G. performed the conductivity and PESA measurements. E. H. performed **2TTN-COFs** BET measurements and edited the manuscript. F. E. and T. F. performed initial mechanochemical optimization screening and edited the manuscript. All other experiments were performed by M. H. G. The manuscript was written by M. H. G. and edited by D. F. P.

Conflicts of interest

There are no conflicts to declare.

Data availability

The data that support the findings of this study are available in the SI of this article and includes synthetic procedures; additional characterization data; a summary of the previously reported thiophene-based COFs, mechanochemically synthesized COFs and COF modifications *via* Doebner reaction; NMR and MS spectra of the COF precursors and model compounds. See DOI: **https://doi.org/10.1039/d5sc04390e**.

Acknowledgements

This work was funded by NSERC of Canada. M. H. G. and F. E. acknowledge support through the FRQNT Doctoral Fellowships. T. F. acknowledges Leverhulme International Professorship (LIP-2021-011) from the Leverhulme Trust and the start-up funds from the University of Birmingham. The authors thank Dr Hatem M. Titi for his help with PXRD analysis and useful discussions; Dr Alexander Wahba and Nadim Saade for the mass spectrometry analysis; Dr Kirill Levin for assistance with EPR measurements and VT NMR; and Petr Fiurasek for support with DRS and IR spectroscopy. The authors appreciate useful discussions with Dr Chang Wan Kang; assistance with the microwave reaction setup from Anaïs Hamelin (Audrey Moores' group) and the support with EIS measurements from Jashanpreet Kaur (Janine Mauzeroll's group).

References

1 K. Geng, T. He, R. Liu, S. Dalapati, K. T. Tan, Z. Li, S. Tao, Y. Gong, Q. Jiang and D. Jiang, Covalent Organic Frameworks: Design, Synthesis, and Functions, *Chem. Rev.*, 2020, **120**, 8814–8933.

2 A. P. Côté, A. I. Benin, N. W. Ockwig, M. O'Keeffe, A. J. Matzger and O. M. Yaghi, Porous, Crystalline, Covalent Organic Frameworks, *Science*, 2005, **310**, 1166–1170.

3 R. Liu, K. T. Tan, Y. Gong, Y. Chen, Z. Li, S. Xie, T. He, Z. Lu, H. Yang and D. Jiang, Covalent organic frameworks: an ideal platform for designing ordered materials and advanced applications, *Chem. Soc. Rev.*, 2021, **50**, 120–242.

4 Q. Gu, X. Lu, C. Chen, X. Wang, F. Kang, Y. Y. Li, Q. Xu, J. Lu, Y. Han, W. Qin and Q. Zhang, High-Performance Piezoelectric Two-Dimensional Covalent Organic Frameworks, *Angew. Chem., Int. Ed.*, 2024, **63**, e202409708.
5 Q. Gu, J. Zha, C. Chen, X. Wang, W. Yao, J. Liu, F. Kang, J. Yang, Y. Y. Li, D. Lei, Z. Tang, Y. Han, C. Tan and Q. Zhang, Constructing Chiral Covalent-Organic Frameworks for Circularly Polarized Light Detection, *Adv. Mater.*, 2024, **36**, 2306414.
6 R. Guntermann, L. Frey, A. Biewald, A. Hartschuh, T. Clark, T. Bein and D. D. Medina, Regioisomerism in Thienothiophene-Based Covalent Organic Frameworks-A Tool for Band-Gap Engineering, *J. Am. Chem. Soc.*, 2024, **146**, 15869–15878.
7 F. Kang, X. Wang, C. Chen, C.-S. Lee, Y. Han and Q. Zhang, Construction of Crystalline Nitrone-Linked Covalent Organic Frameworks Via Kröhnke Oxidation, *J. Am. Chem. Soc.*, 2023, **145**, 15465–15472.
8 M. Calik, F. Auras, L. M. Salonen, K. Bader, I. Grill, M. Handloser, D. D. Medina, M. Dogru, F. Löbermann, D. Trauner, A. Hartschuh and T. Bein, Extraction of Photogenerated Electrons and Holes from a Covalent Organic Framework Integrated Heterojunction, *J. Am. Chem. Soc.*, 2014, **136**, 17802–17807.
9 W. Zhao, P. Yan, B. Li, M. Bahri, L. Liu, X. Zhou, R. Clowes, N. D. Browning, Y. Wu, J. W. Ward and A. I. Cooper, Accelerated Synthesis and Discovery of Covalent Organic Framework Photocatalysts for Hydrogen Peroxide Production, *J. Am. Chem. Soc.*, 2022, **144**, 9902–9909.
10 F. Liu, P. Zhou, Y. Hou, H. Tan, Y. Liang, J. Liang, Q. Zhang, S. Guo, M. Tong and J. Ni, Covalent organic frameworks for direct photosynthesis of hydrogen peroxide from water, air and sunlight, *Nat. Commun.*, 2023, **14**, 4344.
11 Q. Huang, W. Li, Z. Mao, L. Qu, Y. Li, H. Zhang, T. Yu, Z. Yang, J. Zhao, Y. Zhang, M. P. Aldred and Z. Chi, An exceptionally flexible hydrogen-bonded organic framework with large-scale void regulation and adaptive guest accommodation abilities, *Nat. Commun.*, 2019, **10**, 3074.
12 C. G. Gruber, L. Frey, R. Guntermann, D. D. Medina and E. Cortés, Early stages of covalent organic framework formation imaged in operando, *Nature*, 2024, **630**, 872–877.
13 A. Puthukkudi, S. Nath, P. Shee, A. Dutta, C. V. Rajput, S. Bommakanti, J. Mohapatra, M. Samal, S. Anwar, S. Pal and B. P. Biswal, Terahertz Conductivity of Free-Standing 3D Covalent Organic Framework Membranes Fabricated via Triple-Layer-Dual Interfacial Approach, *Adv. Mater.*, 2024, **36**, 2312960.
14 J. Yang, S. Ghosh, J. Roeser, A. Acharjya, C. Penschke, Y. Tsutsui, J. Rabeah, T. Wang, S. Y. Djoko Tameu, M.-Y. Ye, J. Grüneberg, S. Li, C. Li, R. Schomäcker, R. Van De Krol, S. Seki, P. Saalfrank and A. Thomas, Constitutional isomerism of the linkages in donor–acceptor covalent organic frameworks and its impact on photocatalysis, *Nat. Commun.*, 2022, **13**, 6317.
15 Q. Wang, C. Wang, K. Zheng, B. Wang, Z. Wang, C. Zhang and X. Long, Positional Thiophene Isomerization: A Geometric Strategy for Precisely Regulating the Electronic State of Covalent Organic Frameworks to Boost Oxygen Reduction, *Angew. Chem., Int. Ed.*, 2024, **63**, e202320037.
16 P.-J. Tian, X.-H. Han, Q.-Y. Qi and X. Zhao, An Azulene-Based Crystalline Porous Covalent Organic Framework for Efficient Photothermal Conversion, *Small*, 2024, **20**, 2307635.
17 C.-Q. Han, J.-X. Guo, S. Sun, Z.-Y. Wang, L. Wang and X.-Y. Liu, Impact of Imine Bond Orientations and Acceptor Groups on Photocatalytic Hydrogen Generation of Donor–Acceptor Covalent Organic Frameworks, *Small*, 2024, **20**, 2405887.
18 J.-X. Fu, Y. Liu, L.-H. Chen, W.-K. Han, X. Liu, J.-X. Shao, X. Yan and Z.-G. Gu, Positional Isomers of Covalent Organic Frameworks for Indoor Humidity Regulation, *Small*, 2023, **19**, 2303897.
19 T. Wang, M. Li, Y. Chen, X. Che, F. Bi, Y. Yang, R. Yang and C. Li, Regioisomeric Benzotriazole-Based Covalent Organic Frameworks for High Photocatalytic Activity, *ACS Catal.*, 2023, **13**, 15439–15447.
20 Y. Guo, S. Li and M. Shao, Two-Dimensional Covalent Organic Framework Isomers Induce Different Properties, *ACS Appl. Electron. Mater.*, 2024, **6**, 214–220.
21 H. Chen, D. Li, M. Lin, Q. Wang, Y. Zou, J. Ran, Y. Xing and X. Long, Regulating the Isomerization Geometry and Energy State of Covalent Organic Frameworks for Enhanced Oxygen Reduction Activity, *Adv. Mater.*, 2025, **37**, 2500063.
22 W. Song, S. Chen, X. Ren, X. Su, C. Song, Y. Li, L. Chen and F. Bai, Isomeric Covalent Organic Frameworks for High-Efficiency Photocatalytic CO2 Reduction: Substituent Position Effect, *Small*, 2025, **21**, 2409117.
23 B. Feng, X. Chen, P. Yan, S. Huang, C. Lu, H. Ji, J. Zhu, Z. Yang, K. Cao and X. Zhuang, Isomeric Dual-Pore Two-Dimensional Covalent Organic Frameworks, *J. Am. Chem. Soc.*, 2023, **145**, 26871–26882.
24 W. Zhang, M. Sun, J. Cheng, X. Wu and H. Xu, Regulating Electron Distribution in Regioisomeric Covalent Organic Frameworks for Efficient Solar-Driven Hydrogen Peroxide Production, *Adv. Mater.*, 2025, **37**, 2500913.
25 T. P. Kaloni, P. K. Giesbrecht, G. Schreckenbach and M. S. Freund, Polythiophene: From Fundamental Perspectives to Applications, *Chem. Mater.*, 2017, **29**, 10248–10283.
26 M. E. Cinar and T. Ozturk, Thienothiophenes, Dithienothiophenes, and Thienoacenes: Syntheses, Oligomers, Polymers, and Properties, *Chem. Rev.*, 2015, **115**, 3036–3140.
27 G. H. V. Bertrand, V. K. Michaelis, T.-C. Ong, R. G. Griffin and M. Dincă, Thiophene-based covalent organic frameworks, *Proc. Natl. Acad. Sci. U. S. A.*, 2013, **110**, 4923.
28 R. Caballero, B. Cohen and M. Gutiérrez, Thiophene-Based Covalent Organic Frameworks: Synthesis, Photophysics and Light-Driven Applications, *Molecules*, 2021, **26**, 7666–7686.
29 S. Wang, L. Da, J. Hao, J. Li, M. Wang, Y. Huang, Z. Li, Z. Liu and D. Cao, A Fully Conjugated 3D Covalent Organic Framework Exhibiting Band-like Transport with Ultrahigh Electron Mobility, *Angew. Chem., Int. Ed.*, 2021, **60**, 9321–9325.

30 S. Wang, X.-X. Li, L. Da, Y. Wang, Z. Xiang, W. Wang, Y.-B. Zhang and D. Cao, A Three-Dimensional sp2 Carbon-Conjugated Covalent Organic Framework, *J. Am. Chem. Soc.*, 2021, **143**, 15562–15566.

31 Y. Wang, Z. Qiao, H. Li, R. Zhang, Z. Xiang, D. Cao and S. Wang, Molecular Engineering for Modulating Photocatalytic Hydrogen Evolution of Fully Conjugated 3D Covalent Organic Frameworks, *Angew. Chem., Int. Ed.*, 2024, **63**, e202404726.

32 X. Zheng, W. Qiu, J. Cui, H. Liu, Y. Zhao, J. Zhang, Z. Zhang and Y. Zhao, Donor-Acceptor Interactions Enhanced Colorimetric Sensors for Both Acid and Base Vapor Based on Two-Dimensional Covalent Organic Frameworks, *Chem.–Eur. J.*, 2024, **30**, e202303004.

33 S. Hou, G. Liu, H. Gao, H. Li and X. Liang, Highly Efficient Aggregation-induced Electrochemiluminescence Performance of Covalent Organic Frameworks with Electron-rich Conjugated Structures, *Chem.–Eur. J.*, 2025, **31**, e202403820.

34 Y. Liu, H. Zhang, H. Yu, Z. Liao, S. Paasch, S. Xu, R. Zhao, E. Brunner, M. Bonn, H. I. Wang, T. Heine, M. Wang, Y. Mai and X. Feng, A Thiophene Backbone Enables Two-Dimensional Poly(arylene vinylene)s with High Charge Carrier Mobility, *Angew. Chem., Int. Ed.*, 2023, **62**, e202305978.

35 R. Bao, Z. Xiang, Z. Qiao, Y. Yang, Y. Zhang, D. Cao and S. Wang, Designing Thiophene-Enriched Fully Conjugated 3D Covalent Organic Framework as Metal-Free Oxygen Reduction Catalyst for Hydrogen Fuel Cells, *Angew. Chem., Int. Ed.*, 2023, **62**, e202216751.

36 Z.-M. Yang, Y. Wang, M.-H. Zhang, Z.-Y. Hou, S.-P. Zhao, X. Han, S. Yuan, J. Su, Z. Jin and J.-L. Zuo, Electroactive tetrathiafulvalene-based covalent organic framework with thiophene units as anode for high-performance hybrid lithium-ion capacitors: Dedicated to Professor Hong-Cai Zhou on the occasion of his 60th birthday, *Energy Storage Mater.*, 2025, **75**, 104038.

37 H. Wei, J. Ning, X. Cao, X. Li and L. Hao, Benzotrithiophene-Based Covalent Organic Frameworks: Construction and Structure Transformation under Ionothermal Condition, *J. Am. Chem. Soc.*, 2018, **140**, 11618–11622.

38 N. Keller, D. Bessinger, S. Reuter, M. Calik, L. Ascherl, F. C. Hanusch, F. Auras and T. Bein, Oligothiophene-Bridged Conjugated Covalent Organic Frameworks, *J. Am. Chem. Soc.*, 2017, **139**, 8194–8199.

39 T. Sick, J. M. Rotter, S. Reuter, S. Kandambeth, N. N. Bach, M. Döblinger, J. Merz, T. Clark, T. B. Marder, T. Bein and D. D. Medina, Switching on and off Interlayer Correlations and Porosity in 2D Covalent Organic Frameworks, *J. Am. Chem. Soc.*, 2019, **141**, 12570–12581.

40 W. Wang, D. Huang, W. Zheng, X. Zhao, K. He, H. Pang and Y. Xiang, Construction of Amide-Linked Covalent Organic Frameworks by N-Heterocyclic Carbene-Mediated Selective Oxidation for Photocatalytic Dehalogenation, *Chem. Mater.*, 2023, **35**, 7154–7163.

41 J. I. Feldblyum, C. H. McCreery, S. C. Andrews, T. Kurosawa, E. J. G. Santos, V. Duong, L. Fang, A. L. Ayzner and Z. Bao, Few-layer, large-area, 2D covalent organic framework semiconductor thin films, *Chem. Commun.*, 2015, **51**, 13894–13897.

42 B. Cui, X. Zheng, J. Wang, D. Liu, S. Xie and B. Huang, Realization of Lieb lattice in covalent-organic frameworks with tunable topology and magnetism, *Nat. Commun.*, 2020, **11**, 66.

43 A. L. Sharpe, E. J. Fox, A. W. Barnard, J. Finney, K. Watanabe, T. Taniguchi, M. A. Kastner and D. Goldhaber-Gordon, Emergent ferromagnetism near three-quarters filling in twisted bilayer graphene, *Science*, 2019, **365**, 605–608.

44 E. Jin, M. Asada, Q. Xu, S. Dalapati, M. A. Addicoat, M. A. Brady, H. Xu, T. Nakamura, T. Heine, Q. Chen and D. Jiang, Two-dimensional sp2 carbon–conjugated covalent organic frameworks, *Science*, 2017, **357**, 673–676.

45 D. Blätte, F. Ortmann and T. Bein, Photons, Excitons, and Electrons in Covalent Organic Frameworks, *J. Am. Chem. Soc.*, 2024, **146**, 32161–32205.

46 S. Chen, H. Wang, Z. Ou, H. Liu, J. Zhou, P. Hu, Y. Wang, D. Zhong and H. Ji, On-Surface Synthesis of 2D Porphyrin-Based Covalent Organic Frameworks Using Terminal Alkynes, *Chem. Mater.*, 2021, **33**, 8677–8684.

47 T. Friščić, C. Mottillo and H. M. Titi, Mechanochemistry for Synthesis, *Angew. Chem., Int. Ed.*, 2020, **59**, 1018–1029.

48 B. P. Biswal, S. Chandra, S. Kandambeth, B. Lukose, T. Heine and R. Banerjee, Mechanochemical Synthesis of Chemically Stable Isoreticular Covalent Organic Frameworks, *J. Am. Chem. Soc.*, 2013, **135**, 5328–5331.

49 J. Hu, Z. Huang and Y. Liu, Beyond Solvothermal: Alternative Synthetic Methods for Covalent Organic Frameworks, *Angew. Chem., Int. Ed.*, 2023, **62**, e202306999.

50 S. T. Emmerling, L. S. Germann, P. A. Julien, I. Moudrakovski, M. Etter, T. Friščić, R. E. Dinnebier and B. V. Lotsch, In situ monitoring of mechanochemical covalent organic framework formation reveals templating effect of liquid additive, *Chem*, 2021, **7**, 1639–1652.

51 G. Das, D. Balaji Shinde, S. Kandambeth, B. P. Biswal and R. Banerjee, Mechanosynthesis of imine, β-ketoenamine, and hydrogen-bonded imine-linked covalent organic frameworks using liquid-assisted grinding, *Chem. Commun.*, 2014, **50**, 12615–12618.

52 S. Karak, S. Kandambeth, B. P. Biswal, H. S. Sasmal, S. Kumar, P. Pachfule and R. Banerjee, Constructing Ultraporous Covalent Organic Frameworks in Seconds via an Organic Terracotta Process, *J. Am. Chem. Soc.*, 2017, **139**, 1856–1862.

53 E. Hamzehpoor, F. Effaty, T. H. Borchers, R. S. Stein, A. Wahrhaftig-Lewis, X. Ottenwaelder, T. Friščić and D. F. Perepichka, Mechanochemical Synthesis of Boroxine-linked Covalent Organic Frameworks, *Angew. Chem., Int. Ed.*, 2024, **63**, e202404539.

54 D. B. Shinde, H. B. Aiyappa, M. Bhadra, B. P. Biswal, P. Wadge, S. Kandambeth, B. Garai, T. Kundu, S. Kurungot and R. Banerjee, A mechanochemically synthesized covalent organic framework as a proton-conducting solid electrolyte, *J. Mater. Chem. A*, 2016, **4**, 2682–2690.

55 Y. Peng, G. Xu, Z. Hu, Y. Cheng, C. Chi, D. Yuan, H. Cheng and D. Zhao, Mechanoassisted Synthesis of Sulfonated Covalent Organic Frameworks with High Intrinsic Proton Conductivity, *ACS Appl. Mater. Interfaces*, 2016, **8**, 18505–18512.

56 A. Jati, A. K. Mahato, D. Chanda, P. Kumar, R. Banerjee and B. Maji, Photocatalytic Decarboxylative Fluorination by Quinone-Based Isoreticular Covalent Organic Frameworks, *J. Am. Chem. Soc.*, 2024, **146**, 23923–23932.

57 Y. Yang, W. Zhao, H. Niu and Y. Cai, Mechanochemical Construction 2D/2D Covalent Organic Nanosheets Heterojunctions Based on Substoichiometric Covalent Organic Frameworks, *ACS Appl. Mater. Interfaces*, 2021, **13**, 42035–42043.

58 N. Brown, Z. Alsudairy, R. Behera, F. Akram, K. Chen, K. Smith-Petty, B. Motley, S. Williams, W. Huang, C. Ingram and X. Li, Green mechanochemical synthesis of imine-linked covalent organic frameworks for high iodine capture, *Green Chem.*, 2023, **25**, 6287–6296.

59 H. Chen, D. Feng, F. Wei, F. Guo and A. K. Cheetham, Hydrogen-Bond-Regulated Mechanochemical Synthesis of Covalent Organic Frameworks: Cocrystal Precursor Strategy for Confined Assembly, *Angew. Chem., Int. Ed.*, 2024, **64**, e202415454.

60 N. Brown, Q. Zhang, Z. Alsudairy, C. Dun, Y. Nailwal, A. Campbell, C. Harrod, L. Chen, S. Williams, J. J. Urban, Y. Liu and X. Li, Mechanochemical in Situ Encapsulation of Palladium in Covalent Organic Frameworks, *ACS Sustainable Chem. Eng.*, 2024, **12**, 13535–13543.

61 Y. Hu, W.-K. Han, Y. Liu, R.-M. Zhu, X. Yan, H. Pang and Z.-G. Gu, Mechanochemical Transition from a Hydrogen-Bonded Organic Framework to Covalent Organic Frameworks, *ACS Mater. Lett.*, 2023, **5**, 2534–2541.

62 Y. Nailwal, Q. Zhang, N. Brown, Z. Alsudairy, C. Harrod, M. H. Uddin, F. Akram, J. Li, Y. Liu, X. Li and A. Rapid, Sustainable, One-step Mechanochemical Strategy for Synthesizing Gold Nanoparticle-Doped Covalent Organic Frameworks, *Chem.–Eur. J.*, 2025, **31**, e202500339.

63 K. Asokan, M. K. Patil, S. P. Mukherjee, S. B. Sukumaran and T. Nandakumar, Scalable Mechanochemical Synthesis of β-Ketoenamine-linked Covalent Organic Frameworks for Methane Storage, *Chem.–Asian J.*, 2022, **17**, e202201012.

64 S. Hutsch, A. Leonard, S. Grätz, M. V. Höfler, T. Gutmann and L. Borchardt, Mechanochemical Cyclotrimerization: A Versatile Tool to Covalent Organic Frameworks with Tunable Stacking Mode, *Angew. Chem., Int. Ed.*, 2024, **63**, e202403649.

65 J. M. Marrett, F. Effaty, X. Ottenwaelder and T. Friščić, Mechanochemistry for Metal–Organic Frameworks and Covalent–Organic Frameworks (MOFs, COFs): Methods, Materials, and Mechanisms, *Adv. Mater.*, 2025, 2418707, DOI: 10.1002/adma.202418707.

66 Y. Nailwal, B. Baker, Z. Alsudairy, M. El Hariri El Nokab, Q. Zhang, T. Wang, S. Cai, Y. Liu and X. Li, Ambient mechanosynthesis of flexible two-dimensional covalent organic frameworks, *Green Chem.*, 2025, **27**, 8848–8857.

67 C. Zou, Q. Li, Y. Hua, B. Zhou, J. Duan and W. Jin, Mechanical Synthesis of COF Nanosheet Cluster and Its Mixed Matrix Membrane for Efficient CO2 Removal, *ACS Appl. Mater. Interfaces*, 2017, **9**, 29093–29100.

68 J.-J. Liu, J. Yang, J.-L. Wang, Z.-F. Chang, B. Li, W.-T. Song, Z. Zhao, X. Lou, J. Dai and F. Xia, Tetrathienylethene based red aggregation-enhanced emission probes: super red-shifted mechanochromic behavior and highly photostable cell membrane imaging, *Mater. Chem. Front.*, 2018, **2**, 1126–1136.

69 L. Liu, B. Yang, T. J. Katz and M. K. Poindexter, Improved methodology for photocyclization reactions, *J. Org. Chem.*, 1991, **56**, 3769–3775.

70 L. Viglianti, N. L. C. Leung, N. Xie, X. Gu, H. H. Y. Sung, Q. Miao, I. D. Williams, E. Licandro and B. Z. Tang, Aggregation-induced emission: mechanistic study of the clusteroluminescence of tetrathienylethene, *Chem. Sci.*, 2017, **8**, 2629–2639.

71 A. Yamamoto, E. Ohta, N. Kishigami, N. Tsukahara, Y. Tomiyori, H. Sato, Y. Matsui, Y. Kano, K. Mizuno and H. Ikeda, Synthesis and basic properties of tetrathieno[2,3-a:3′,2′-c:2″,3″-f:3‴,2‴-h]naphthalene: a new π-conjugated system obtained by photoinduced electrocyclization–dehydrogenation reactions of tetra(3-thienyl)ethene, *Tetrahedron Lett.*, 2013, **54**, 4049–4053.

72 T. Friščić, S. L. Childs, S. A. A. Rizvi and W. Jones, The role of solvent in mechanochemical and sonochemical cocrystal formation: a solubility-based approach for predicting cocrystallisation outcome, *CrystEngComm*, 2009, **11**, 418–426.

73 A. Yamamoto, Y. Matsui, T. Asada, M. Kumeda, K. Takagi, Y. Suenaga, K. Nagae, E. Ohta, H. Sato, S. Koseki, H. Naito and H. Ikeda, Amorphous Solid Simulation and Trial Fabrication of the Organic Field-Effect Transistor of Tetrathienonaphthalenes Prepared by Using Microflow Photochemical Reactions: A Theoretical Calculation-Inspired Investigation, *J. Org. Chem.*, 2016, **81**, 3168–3176.

74 M. R. Rao, Y. Fang, S. De Feyter and D. F. Perepichka, Conjugated Covalent Organic Frameworks via Michael Addition–Elimination, *J. Am. Chem. Soc.*, 2017, **139**, 2421–2427.

75 L. Cusin, H. Peng, A. Ciesielski and P. Samorì, Chemical Conversion and Locking of the Imine Linkage: Enhancing the Functionality of Covalent Organic Frameworks, *Angew. Chem., Int. Ed.*, 2021, **60**, 14236–14250.

76 J. L. Segura, S. Royuela and M. Mar Ramos, Post-synthetic modification of covalent organic frameworks, *Chem. Soc. Rev.*, 2019, **48**, 3903–3945.

77 F. Haase, E. Troschke, G. Savasci, T. Banerjee, V. Duppel, S. Dörfler, M. M. J. Grundei, A. M. Burow, C. Ochsenfeld, S. Kaskel and B. V. Lotsch, Topochemical conversion of an imine- into a thiazole-linked covalent organic framework enabling real structure analysis, *Nat. Commun.*, 2018, **9**, 2600.

78 Y. Yang, L. Yu, T. Chu, H. Niu, J. Wang and Y. Cai, Constructing chemical stable 4-carboxyl-quinoline linked

covalent organic frameworks via Doebner reaction for nanofiltration, *Nat. Commun.*, 2022, **13**, 2615.

79 P. Das, G. Chakraborty, J. Roeser, S. Vogl, J. Rabeah and A. Thomas, Integrating Bifunctionality and Chemical Stability in Covalent Organic Frameworks via One-Pot Multicomponent Reactions for Solar-Driven H2O2 Production, *J. Am. Chem. Soc.*, 2023, **145**, 2975–2984.

80 E. Jin, K. Geng, K. H. Lee, W. Jiang, J. Li, Q. Jiang, S. Irle and D. Jiang, Topology-Templated Synthesis of Crystalline Porous Covalent Organic Frameworks, *Angew. Chem., Int. Ed.*, 2020, **59**, 12162–12169.

81 D. B. Patel, D. P. Rajani, S. D. Rajani and H. D. Patel, A green synthesis of quinoline-4-carboxylic derivatives using p-toluenesulfonic acid as an efficient organocatalyst under microwave irradiation and their docking, molecular dynamics, ADME-Tox and biological evaluation, *J. Heterocycl. Chem.*, 2020, **57**, 1524–1544.

82 G. C. Muscia, J. P. Carnevale, M. Bollini and S. E. Asís, Microwave-assisted döbner synthesis of 2-phenylquinoline-4-carboxylic acids and their antiparasitic activities, *J. Heterocycl. Chem.*, 2008, **45**, 611–614.

83 R. Gutzler and D. F. Perepichka, π-Electron Conjugation in Two Dimensions, *J. Am. Chem. Soc.*, 2013, **135**, 16585–16594.

84 E. Hamzehpoor, P. Ghamari, Y. Tao, M. G. Rafique, Z. Zhang, M. Salehi, R. S. Stein, J. Ramos-Sanchez, A. W. Laramée, G. Cosa, C. Pellerin, A. Seifitokaldani, R. Z. Khaliullin and D. F. Perepichka, Azatriangulene-Based Conductive C═C Linked Covalent Organic Frameworks with Near-Infrared Emission, *Adv. Mater.*, 2024, **36**, 2413629.

85 S. Chandra, T. Kundu, S. Kandambeth, R. BabaRao, Y. Marathe, S. M. Kunjir and R. Banerjee, Phosphoric Acid Loaded Azo (–N═N–) Based Covalent Organic Framework for Proton Conduction, *J. Am. Chem. Soc.*, 2014, **136**, 6570–6573.

86 X. Meng, H.-N. Wang, S.-Y. Song and H.-J. Zhang, Proton-conducting crystalline porous materials, *Chem. Soc. Rev.*, 2017, **46**, 464–480.

87 T. Jadhav, Y. Fang, C.-H. Liu, A. Dadvand, E. Hamzehpoor, W. Patterson, A. Jonderian, R. S. Stein and D. F. Perepichka, Transformation between 2D and 3D Covalent Organic Frameworks via Reversible [2 + 2] Cycloaddition, *J. Am. Chem. Soc.*, 2020, **142**, 8862–8870.

88 Y. Yang, X. He, P. Zhang, Y. H. Andaloussi, H. Zhang, Z. Jiang, Y. Chen, S. Ma, P. Cheng and Z. Zhang, Combined Intrinsic and Extrinsic Proton Conduction in Robust Covalent Organic Frameworks for Hydrogen Fuel Cell Applications, *Angew. Chem., Int. Ed.*, 2020, **59**, 3678–3684.